Integration of Spaceborne LiDAR and Imaging Spectroscopy in Vegetation Classification

Undergraduate Thesis

Presented in Partial Fulfillment of the Requirements for Graduation with Research Distinction in the College of Engineering

The Ohio State University
Department of Food, Agricultural, and Biological Engineering
Spring 2021

Presented by
James Cross

Undergraduate Thesis Committee
Darren Drewry, Advisor
Gil Bohrer

Abstract

In the face of a dramatically changing climate, the need to model, monitor, and respond to our environment has never been greater or so nearly within our grasps. Advances in remote sensing have made possible the rise of automated methods to study vegetation at a fine detail over previously unimaginable scales. The 2018 launch of the DLR Earth Sensing Imaging Spectrometer (DESIS) coincided with the beginning of NASA's Global Ecosystem Dynamic Investigation (GEDI) mission. For the first time, high resolution spaceborne LiDAR (GEDI) was onboard the International Space Station (ISS) in tandem with hyperspectral imaging instrumentation (DESIS). This occasion presents a unique opportunity in remote sensing to obtain temporally-proximal spectral and structural information from spaceborne sources. Through the integration of these two data sources, we constructed a random forest classification model to perform successional classification on three classes over a study site in upper Michigan. The classifier was trained over distinct datasets from each instrument, then over a combined dataset utilizing data from both instruments. Over this combined dataset, the model achieved 91.7% classification accuracy, greater than the 80.2% and 88.6% accuracies achieved from either instrument in isolation. These results suggest predictive variation between spectral imaging and structural information from LiDAR can be determined algorithmically as in a random forest classifier.

Acknowledgements

My utmost thanks and gratitude go to my advisor Dr. Darren Drewry for guiding me through the research process and assisting me in my journey to graduate school. This project has been a journey in and of its own, shifting and morphing as we worked through it, always finding new and interesting topics within. Without his support, this research would not have taken place and I would be on a vastly different path than I am now. I'm sincerely grateful for his guidance.

Additional thanks go to the College of Engineering Undergraduate Research Program for arranging a point of contact with Dr. Drewry and providing funding in the form of an Undergraduate Research Scholarship that has made this project feasible.

Table of Contents

List of Figures

Introduction

Carbon sequestration in forests is a vital process wherein vegetation uptakes atmospheric carbon dioxide through photosynthesis. In a globally warming climate driven by carbon emissions, our future critically depends on our knowledge of carbon exchange within Earth's biosphere (Berry & Frankenberg, n.d.). The nature of this exchange is governed by variations in plant functional characteristics and remains an ongoing field of study (Asner et al., 2015). Over longer time-scale ecological succession dynamics drive forest development and carbon exchange, requiring a greater degree of understanding of successional states (Falkowski et al., 2009). Traditional field studies are increasingly inadequate for the large scale studies needed in modern studies, now serving as validation for remote sensing methods. Satellite based remote sensing methods are now capable of measuring swaths of the Earth's surface, providing an unprecedented availability of data products. Accurate means of retrieving usable information from these products are therefore needed to develop our understanding of carbon dynamics.

Airborne observational campaigns have provided an opportunity to characterize vegetation structure by way of light detection and ranging (LiDAR) instruments, and biochemistry through imaging spectroscopy (IS). These campaigns however are limited in the extent of the spatial domain covered, and the combination of LiDAR and IS together within close temporal proximity is very rare, making it difficult to quantify the combined information in LiDAR and IS observations for understanding terrestrial vegetation. The spectral reflectance values often relied on by IS methods are strongly influenced by underlying vegetative structure, suggesting a codependence of spatially and temporally available spectral and structural measurements (Knyazikhin et al., 2013). Space-borne IS availability far exceeds that of LiDAR, leaving structural information as the constraining factor.

Historically, satellite based instruments have focused on passive methods such as canopy cover products and spectral imaging. Maps of forest cover have been versatile tools, though they suffer from limited ability to differentiate subtle changes and low sensitivity in heavily-forested regions (Tang et al., 2019). Spaceborne LiDAR promises to fill the widespread gap in observations of forest canopy structure. NASA's Global Ecosystem and Dynamics Investigation (GEDI) LiDAR instrument onboard the International Space Station is the first instance of spaceborne LiDAR designed to study forest vertical structure (Dubayah et al., 2020). The 25m footprint acquisitions made by GEDI are received as waveforms encoding 3D spatial information through vertical profiles, as well as canopy height, cover fraction, elevation, and additional products. Validated empirical models and machine-learning techniques facilitate the conversion from raw waveforms to higher level data products (Dubayah et al., 2020; Lang et al., 2020).

Canopy cover and height are two products that have been frequently used to identify successional stages in temperate forests (Falkowski et al., 2009); however, newer metrics of vertical structure consistently provide better predictors in classification models (Bergen et al., 2009). Plant area volume density (PAVD) is a vertical profile metric, measuring the net plant surface area per unit volume vertically resolved through the canopy. PAVD derived from airborne LiDAR has been used in tropical forests to classify rainforest and eucalypt stand types with an overall 84% accuracy across four classes (Fedrigo et al., 2018). Classification accuracy is fundamentally limited by an expectation of variability when solely using vertical structure information, a limitation in mixed forests. Variation in species and successional states within a forest introduce overlapping canopy distributions, requiring additional field measurements (Marselis et al., 2018). We introduce successional land-cover classifications maps and spectral

imaging acquisitions to overcome these limitations and as a means of validating our classifications.

Imaging spectrometers are instruments used to measure the relative intensity of light reflected from the Earth's surface. The DLR Earth Sensing Imaging Spectrometer (DESIS) acquires continuous hyperspectral reflectance images over the visible through near infrared (VNIR), 400 to 1000 nm, spectral domain at a spatial resolution of 30m and over 235 spectral bands (Alonso et al., 2019). Spectral bands have been used in vegetative indices to model relationships between reflectance values and better understand features of underlying vegetation. The normalized vegetation difference index (NDVI) forms a relationship between near-infrared light and visible light to determine the degree of vegetation growth and carbon sequestration (Jeong et al., 2017). Further, several indices have been developed to act as measures of chlorophyll content, utilizing three or four wavelengths' reflectance values in their calculations (Haboudane et al., 2002). The success of these narrow-band indices has been driven by technological advancements in spectrometers, such as DESIS, though they are still constrained in accuracy by a necessary understanding of structural variation and composition of the site (Ustin et al., 2009). In the last few years a significant opportunity has opened up to utilize the combined structural and spectral information in LiDAR and IS through instrument deployments to the International Space Station (ISS).

Coordinated planning of the GEDI and DESIS instruments allows temporally-proximate acquisitions of both spectral and structural information. Typical vegetative indices include fewer than four wavelengths in their calculation. Utilization of the full spectral and structural profiles would provide a more complete description, but introduces a high dimensional input classification problem. Random Forest (RF) classification trees are commonly used algorithms in

remote sensing that have achieved high accuracy over spectral and structural data sources ((Chan & Paelinckx, 2008; Falkowski et al., 2009; Lawrence et al., 2006). RF trees combine multiple classifiers to avoid overfitting, achieve reliable performance, and improve accuracy over any single classifier approach. In addition, RF trees are capable of identifying the importance of individual variables, a pertinent feature that may be used in determining the dependence over specific structural or spectral characteristics.

In this study we seek to integrate GEDI and DESIS acquisitions as two synergistic sources of information on vegetation structure and function to quantify their respective and combined capabilities to differentiate successional stages in a mixed forest system through a Random Forest classifier. The chosen site for this study is the University of Michigan Biological Station (UMBS), a mixed species forest in upper Michigan. The UMBS site is part of a large-scale experimental disturbance to identify how disturbance and succession influence carbon flux in mixed temperate forests (Gough et al., 2012). It is through this site, and experimentation wherein, that we base our findings on the accuracy and feasibility of our approach.

Methodology

Study Site

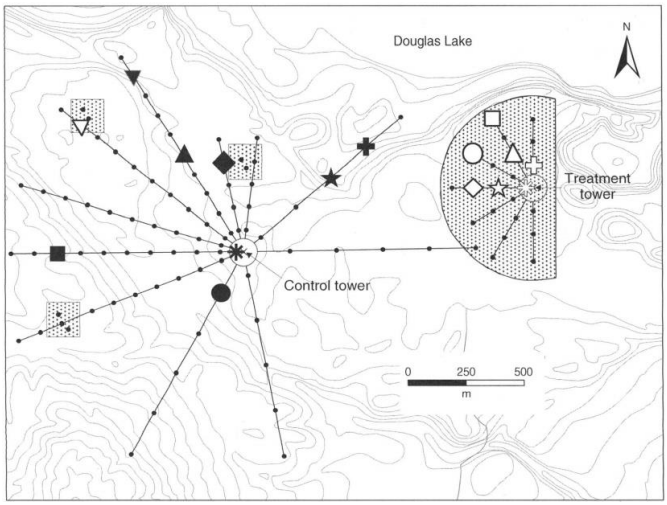

Figure 1. UMBS Flux Tower Plot. Market area around the treatment tower indicates disturbed forest region. Sourced from (Gough et al., 2012)

The UMBS study site (45°56’ N, 84°69’ W) consists predominantly of Aspen and Birch species, with relative compositions of 35% Aspen and Birch, 20% Red Oak, 20% Red Maple, and 35% mixed species, totaling nearly 1300 ha. In 2008, an experimental disturbance was initiated at the site within a 39-ha region surrounding one of the two meteorological towers at the site. The disturbed region underwent stem-girdling of Aspen and Birch species. Defoliation as a result of girdling accelerated mortality of these species in a manner comparable to insects and disease. As a result, Red Oak and Red Maple overtook the disturbed region with a distribution of 40% Red Oak, 40% Red Maple, and 20% mixed species (Gough et al., 2012). The two meteorological towers at the site provide continuous measurement of temperature, humidity, heat flux, and CO2 concentrations throughout the canopy (Figure 1).

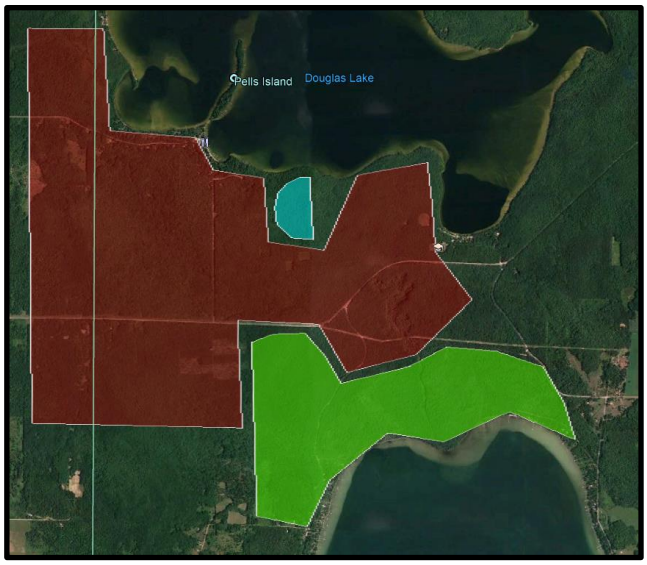

Figure 2. Successional Classification Scheme over UMBS. Undisturbed Forests (Red), Disturbed Forests (Blue), Coniferous Forests (Green)

Forest composition throughout the UMBS study site is consistent with variation occurring gradually outside of the disturbed region. A homogenous coniferous forest occurs off-site, to the southeast of the meteorological towers and within reasonable distance of the site. With these distinctions, a classification scheme of three successional stages was constructed for this study: undisturbed forests, disturbed forests, and coniferous forests. Plot specifications from UMBS (Gough et al., 2012) along with LANDSAT imagery were used to produce a land cover map of the three successional stages (Figure 2). Undisturbed forests represent the largest region, occupying all areas not covered by the coniferous forest region or the disturbance plot. This map is used as the ground truth classification for our acquisitions over the site.

GEDI

Vertical structural information was obtained in the form of PAVD profiles as a Level 2B data product from the GEDI Instrument. The sole observable of the GEDI Instrument is the returned LiDAR waveform, from which additional metrics are derived. GEDI measurements are made across 8 parallel laser tracks, transects, simultaneously following the ground reference

tracks of the ISS from an altitude of 410km. Each measurement is a geolocated 25m diameter footprint separated by 35m along track, and 600m between tracks. PAVD is calculated as one half of the estimated plant surface area per unit volume. A 5m height step is used, up to a maximum height of 50m, creating a profile of 10 PAVD measurements (Dubayah et al., 2020).Variation in PAVD profiles predominantly occurs in the lower 20m of the profile (Figure 3).

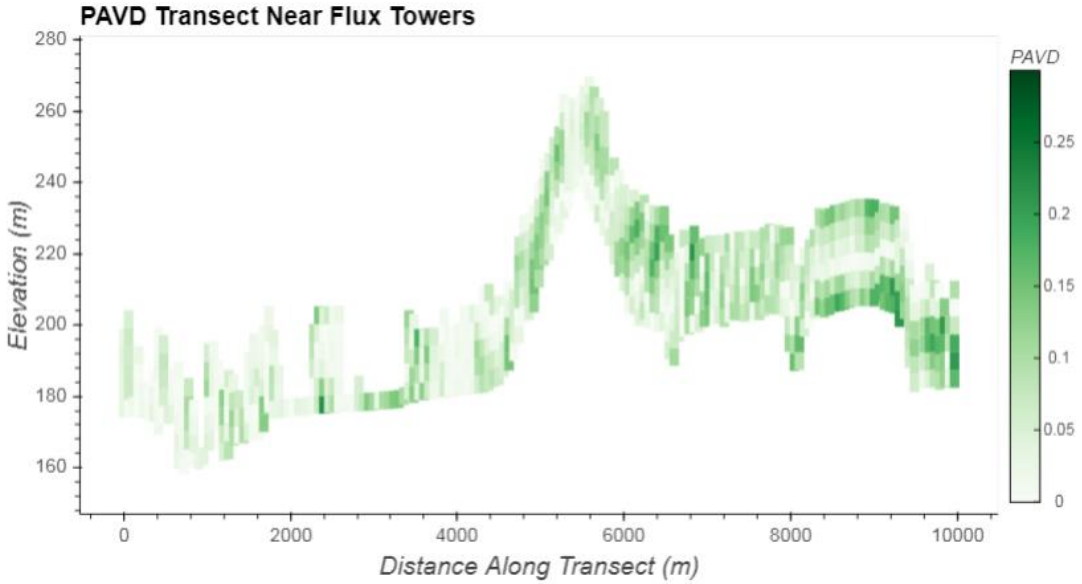

Figure 3. Sample PAVD Profile Transect over UMBS

As of April 2021, 29 instances of Level 2B data products have been processed and made available over the UMBS region, irregularly acquired between May 2019 and August 2020. Spatial subsetting of acquisitions over UMBS was performed as part of the initial acquisition of data from NASA's Earthdata service. Further filtering was performed based on values of the L2B Quality Flag product, a provided product derived from lower level product flags as well as methods in the GEDI L2B algorithm. Remaining data consists of high-quality individual footprints with associated PAVD profiles and geolocated positions. Footprints that were found to

intersect successional classifications regions were labeled accordingly to produce 588 classified data points (Figure 4).

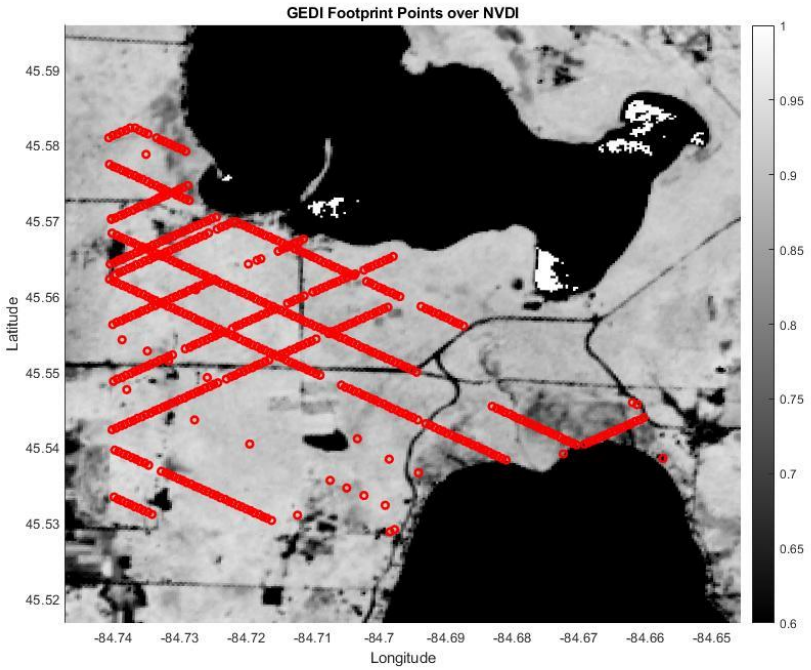

Figure 4. GEDI Footprint Locations over UMBS. Surface colorized by NDVI calculated over August 11th DESIS acquisition.

DESIS

Spectral acquisitions of the site were located in the summer of 2020 from the DESIS instrument. DESIS is a hyperspectral instrument operating over the 400nm to 1000nm spectral domain, VNIR, at a spatial resolution of 30m and 2.55nm average bin width (Alonso et al., 2019). Acquisitions have a coverage of 30km x 30km, corresponding to 1024 x 1024 pixels. Surface reflectance products undergo orthorectification and atmospheric compensation to reduce image distortion in Level 2A processing. Reflectance values in each of the 235 spectral bins are scaled by a gain factor and stored as an integer, with specifications provided to recover the original data.

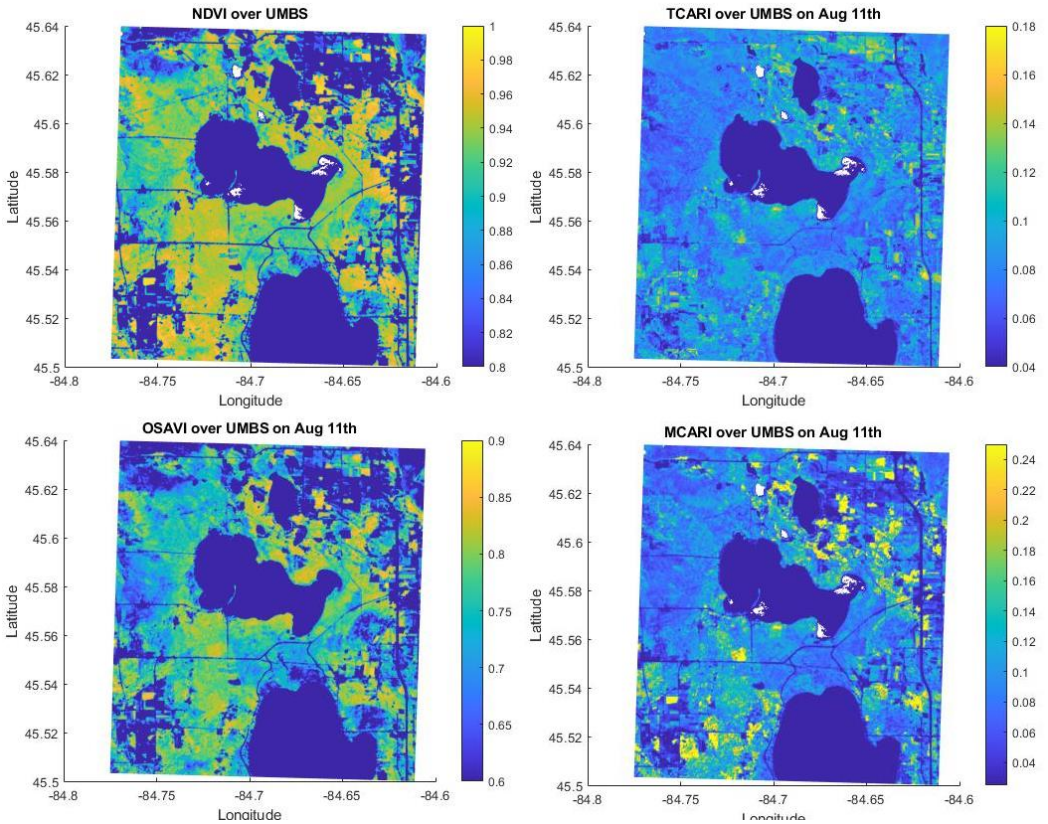

Figure 5. Four Vegetative Indices over UMBS, calculated over August 11th DESIS acquisition.

Five acquisitions were made over the UMBS region and three were suitably clear of cloud cover for use in this study. These acquisitions occurred on July 3rd, August 7th, and August 11th of 2020. Images were converted to reflectance plots and subsequently filtered for data points labeled low-quality. A projection from the provided reference points was performed to produce a gridded georeference matrix underlying individual pixels in the surface reflectance product. With this grid, the latitude and longitude positions of individual pixels was known, allowing direct comparison across the three acquisitions. Each acquisition was subset over the UMBS region and co-aligned to a common reference grid. Fusion of GEDI footprints and DESIS pixels was performed by selection of the nearest pixels with no additional aggregation taking place. Further filtering was performed to remove reflectance spectra corresponding to non-

vegetative surfaces, such as structures, roads, or water surfaces. Remaining reflectance spectra are presented in Figures 6 and 7, colored by successional classification.

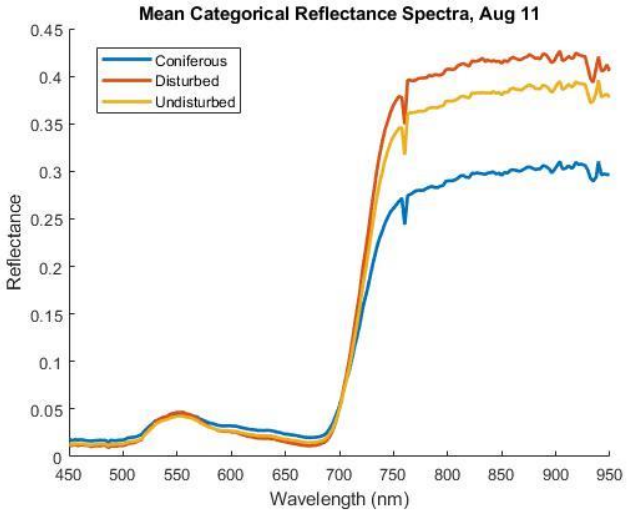

Figure 6. Mean spectra from classified footprints over UMBS on August 11th DESIS acquisition

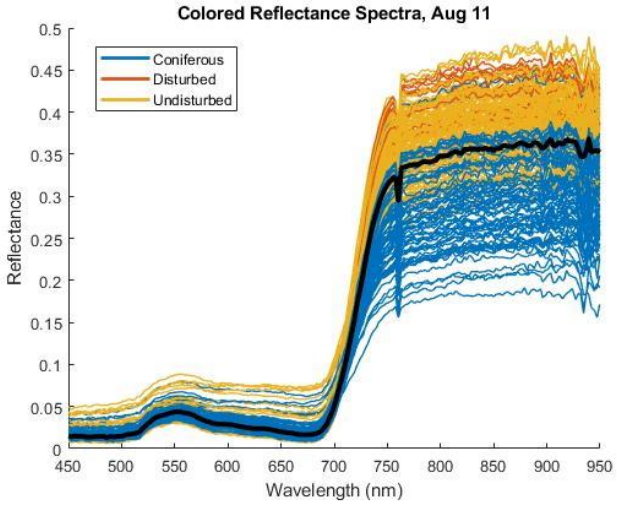

Figure 7. All reflectance spectra colorized by classification from August 11th DESIS acquisition

Classification and Validation

In Random Forest (RF) classification, tree splits occur over random subsets of the input feature vector. At each split, multiple classification models are tested over randomized sets of the training data, with each decision decided by majority vote of the training instances. Although RF provides a greatly reduced need for parameterization over other models, an automated approach was taken to select optimal hyperparameters for the number of learning cycles and leaf size (Pal, 2005).

Utilizing MATLAB's Statistics and Machine Learning Toolbox, the data from DESIS, GEDI, and the land classification was combined into a single feature vector for all 588 data points. Spectra from separate DESIS acquisitions are considered separately due to temporal differences that may affect the underlying vegetation and presence of overlapping maps. Availability of PAVD profiles were the limiting factor of data points. Separation of GEDI

footprints ensures no overlap of measurements, allowing only one PAVD profile for each data point. The input feature vector is composed of 715 elements corresponding to the 3 reflectance spectra acquisitions of 235 bands each, and the 10 element PAVD profile.

A random forest classifier was developed to learn and predict successional classification over UMBS. The classifier was trained using a K-Fold cross-validation algorithm, with an initial 50% holdout validation set, over three sets of data to determine the information content of each data source for classifying successional at UMBS: PAVD profiles, VNIR reflectance spectra, and the combination of both data sets. To verify repeatability of this approach, each set was trained over 10 iterations, providing a method to calculate mean and standard deviation of the model. From the constructed RF trees, MATLAB provides methods to estimate feature prediction importance through permutation of inputs. Higher importance scores indicate a greater response of the model due to variation in that particular feature.

Results

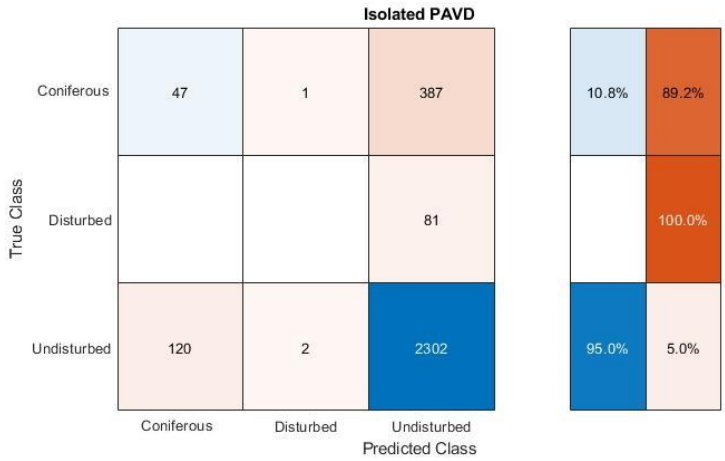

Figure 8. Isolated PAVD Training Confusion Chart

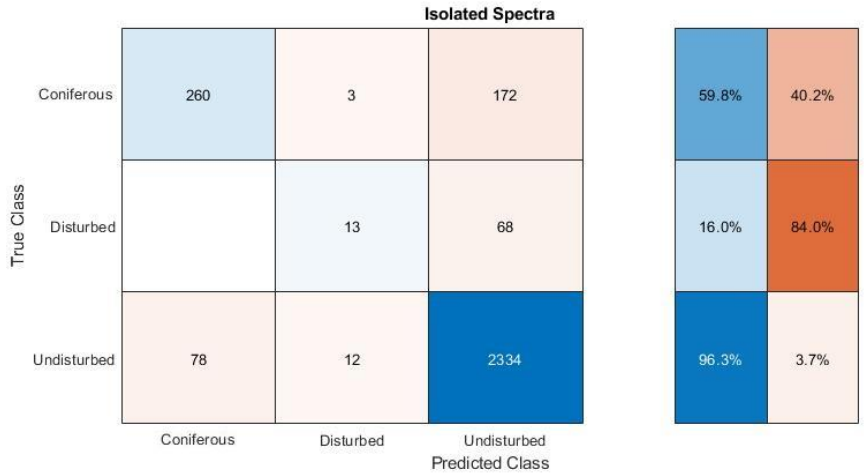

Figure 10. Isolated Training over Spectra Confusion Chart

Figure 12. Complete Dataset Training Confusion Chart

Hyperparameter optimization was performed over the calibration data to determine the optimal number of learning cycles and leaf sizes, identifying 473 cycles and a minimum leaf size of 1 as the most optimal parameters over the dataset. We maintained these parameters through all iterations of training data. In the first iteration, training was restricted to PAVD profiles with an overall reported accuracy of 80.2% over the training data. Misclassification occurred most strongly in the disturbed classification; all instances of disturbed forests were misclassified as undisturbed forests. Identification of coniferous forests had an accuracy of 10.1%, whereas

undisturbed forests had an accuracy of 95.6% (Figure 8). Misclassification tended toward identification as undisturbed forests, the majority class. PAVD profile segments 5 and 1, corresponding to height segments 25m-30m and 0m-5m respectively, were identified as the most important features in predicting successional classification (Figure 9).

The focus of the second training iteration was isolation of spectral data. Classifying over the full 235 bin reflectance spectra reported an overall accuracy of 88.6%. Classification over all classes improved over PAVD training with coniferous forests at 59.8%, disturbed forests at 16%, and undisturbed forests at 96.3% accuracy (Figure 10). The strongest individual predictors occur in bins 203 and 33, centered over wavelengths at 918nm and 483nm. Overall predictor strength increases near edges of the region and in the central region, near 700nm (Figure 11).

Training the classifier over the combined feature vector of all three spectral profiles and the PAVD profile produced the highest accuracy at 91.7%. Classification accuracies of coniferous forests and undisturbed forests increased to 67.8% and 98.5% respectively (Figure 12). Unexpectedly, prediction accuracy of disturbed forests was lower than training on spectral data alone, with an accuracy of 12.3%. Predictor importance varied from previous tests. The predominant predictor was a spectral bin centered on 447nm, corresponding to the July 3rd DESIS acquisition (Figure 13).

Discussion

Throughout the study a number of expected and unexpected effects were observed. Significant improvement is observed across the three iterations of training. Performing classification over structural data and spectral data, individually, produced accuracies of 80.2% and 88.6% respectively. The combined product outperformed both individual products with an

accuracy of 91.7%, increasing the overall accuracy, but decreasing accuracy in the disturbed forest classification over the classifier trained on spectral data. Although the random forests algorithm is robust, flexible, and simple to use, it has low sensitivity to hyperparameter selection and is difficult to tune (Lawrence et al., 2006). In all iterations of training there exists a large discrepancy in classification accuracy across the three successional stages. Undisturbed forests are consistently the most well-classified, as a result of accounting for 82% of data points, while disturbed forests performed the worst and account for only 2.9% of the total dataset. Low sample size was likely a primary contributor to misclassification rates due to the data-driven approach of the random forests algorithm.

An 80.2% classification accuracy was achieved in the classification of successional stages utilizing only structural information. Fedrigo (2018) reported a similar accuracy of 83.8% utilizing principle component analysis in conjunction with random forests to identify four successional classes in tropical forests. The PAVD profiles used in their study had a spatial resolution of 1m, finer than the 5m profiles provided by GEDI. In addition, the GEDI PAVD profiles obtained over UMBS often do not contain information in their highest levels. Figure 9 depicts this pattern by indicating a low prediction importance across the four highest bins in the profile.

The classifier trained on the fusion of PAVD profiles and spectral data performed with an accuracy of 91.7%. This degree of accuracy is comparable to, or exceeding, those achieved in similar studies focused on successional classification using spectral data: 94% (Thenkabil et al., 2004), 93% (Lawrence et al., 2006), and 65% (Chan & Paelinckx, 2008). Results between these studies are not directly comparable due to differences in ecosystem domain, specificity of

successional classification, and availability of data. Further, the accuracy of the classifier in this study was biased by a heavily-skewed classification distribution.

Another shortcoming of this study was an incompatibility in instrumentation to our study site. The GEDI Instrument operates to equally space acquisitions along the Earth's surface, however, the disturbance site is significantly dwarfed by the undisturbed and coniferous sites, and is an exceptionally small region for the GEDI Instrument to observe. Further study of this particular site may benefit from targeted methods using airborne LiDAR.

Due to the numerical methods used here, the findings of this approach may be limited to comparable ecosystems as that found at UMBS (Asner et al., 2015). However, the data products used within were chosen due to their synergy and global coverage, and so the methods and software are flexible enough to allow sampling from a much larger range of sites. Future studies should consider further processing of spectral data or PAVD profiles, such as PCA, to improve predictive results and reduce computation time.

Conclusion

In this study we have demonstrated the feasibility of combining biochemical and structural information from spaceborne instrumentation for the purpose of characterizing successional stages in upper Michigan. The methods and data products chosen for this study are generalizable to regions with limited field access where successional classification has been established. Data products from GEDI and DESIS instrumentation were used to classify three successional classifications with an overall accuracy of 91.7%. In future studies, a larger data site with equal representation of successional stages would complement the strengths of spaceborne acquisitions.

References

01. Asner, G. P., Martin, R. E., Anderson, C. B., & Knapp, D. E. (2015). Quantifying forest canopy traits: Imaging spectroscopy versus field survey. *Remote Sensing of Environment*, *158*, 15–27. https://doi.org/10.1016/j.rse.2014.11.011

02. Alonso, K., Bachmann, M., Burch, K., Carmona, E., Cerra, D., de los Reyes, R., Dietrich, D., Heiden, U., Hölderlin, A., Ickes, J., Knodt, U., Krutz, D., Lester, H., Müller, R., Pagnutti, M., Reinartz, P., Richter, R., Ryan, R., Sebastian, I., & Tegler, M. (2019). Data Products, Quality and Validation of the DLR Earth Sensing Imaging Spectrometer (DESIS). *Sensors*, *19*(20), 4471. https://doi.org/10.3390/s19204471

03. Bergen, K. M., Goetz, S. J., Dubayah, R. O., Henebry, G. M., Hunsaker, C. T., Imhoff, M. L., Nelson, R. F., Parker, G. G., & Radeloff, V. C. (2009). Remote sensing of vegetation 3-D structure for biodiversity and habitat: Review and implications for lidar and radar spaceborne missions. *Journal of Geophysical Research: Biogeosciences*, *114*(G2). https://doi.org/10.1029/2008JG000883

04. Berry, J., & Frankenberg, C. (n.d.). *New Methods for Measurements of Photosynthesis from Space*. 72.

05. Chan, J. C.-W., & Paelinckx, D. (2008). Evaluation of Random Forest and Adaboost tree-based ensemble classification and spectral band selection for ecotope mapping using airborne hyperspectral imagery. *Remote Sensing of Environment*, *112*(6), 2999–3011. https://doi.org/10.1016/j.rse.2008.02.011

06. Dubayah, R., Blair, J. B., Goetz, S., Fatoyinbo, L., Hansen, M., Healey, S., Hofton, M., Hurtt, G., Kellner, J., Luthcke, S., Armston, J., Tang, H., Duncanson, L., Hancock, S., Jantz, P., Marselis, S., Patterson, P. L., Qi, W., & Silva, C. (2020). The Global Ecosystem Dynamics Investigation: High-resolution laser ranging of the Earth's forests and

topography. *Science of Remote Sensing*, *1*, 100002. https://doi.org/10.1016/j.srs.2020.100002

07. Falkowski, M. J., Evans, J. S., Martinuzzi, S., Gessler, P. E., & Hudak, A. T. (2009). Characterizing forest succession with lidar data: An evaluation for the Inland Northwest, USA. *Remote Sensing of Environment*, *113*(5), 946–956. https://doi.org/10.1016/j.rse.2009.01.003
08. Fedrigo, M., Newnham, G. J., Coops, N. C., Culvenor, D. S., Bolton, D. K., & Nitschke, C. R. (2018). Predicting temperate forest stand types using only structural profiles from discrete return airborne lidar. *ISPRS Journal of Photogrammetry and Remote Sensing*, *136*, 106–119. https://doi.org/10.1016/j.isprsjprs.2017.11.018
09. Gough, C. M., Hardiman, B. S., Nave, L. E., Bohrer, G., Maurer, K. D., Vogel, C. S., Nadelhoffer, K. J., & Curtis, P. S. (2013). Sustained carbon uptake and storage following moderate disturbance in a Great Lakes forest. *Ecological Applications*, *23*(5), 1202–1215.
10. Haboudane, D., Miller, J. R., Tremblay, N., Zarco-Tejada, P. J., & Dextraze, L. (2002). Integrated narrow-band vegetation indices for prediction of crop chlorophyll content for application to precision agriculture. Remote Sensing of Environment, 81(2–3), 416–426. https://doi.org/10.1016/S0034-4257(02)00018-4
11. Jeong, S.-J., Schimel, D., Frankenberg, C., Drewry, D. T., Fisher, J. B., Verma, M., Berry, J. A., Lee, J.-E., & Joiner, J. (2017). Application of satellite solar-induced chlorophyll fluorescence to understanding large-scale variations in vegetation phenology and function over northern high latitude forests. *Remote Sensing of Environment*, *190*, 178–187. https://doi.org/10.1016/j.rse.2016.11.021

12. Knyazikhin, Yuri, Mitchell A. Schull, Pauline Stenberg, Matti Mõttus, Miina Rautiainen, Yan Yang, Alexander Marshak, et al. "Hyperspectral Remote Sensing of Foliar Nitrogen Content." *Proceedings of the National Academy of Sciences* 110, no. 3 (January 15, 2013): E185–92. https://doi.org/10.1073/pnas.1210196109.
13. Lang, N., Kalischek, N., Armston, J., Schindler, K., Dubayah, R., & Wegner, J. D. (2021). Global canopy height estimation with GEDI LIDAR waveforms and Bayesian deep learning. *ArXiv:2103.03975 [Physics]*. http://arxiv.org/abs/2103.03975
14. Lawrence, R. L., Wood, S. D., & Sheley, R. L. (2006). Mapping invasive plants using hyperspectral imagery and Breiman Cutler classifications (randomForest). *Remote Sensing of Environment*, *100*(3), 356–362. https://doi.org/10.1016/j.rse.2005.10.014
15. Marselis, S. M., Tang, H., Armston, J., Abernethy, K., Alonso, A., Barbier, N., Bissiengou, P., Jeffery, K., Kenfack, D., Labrière, N., Lee, S.-K., Lewis, S. L., Memiaghe, H., Poulsen, J. R., White, L., & Dubayah, R. (2019). Exploring the relation between remotely sensed vertical canopy structure and tree species diversity in Gabon. *Environmental Research Letters*, *14*(9), 094013. https://doi.org/10.1088/1748-9326/ab2dcd
16. Marselis, S. M., Tang, H., Armston, J. D., Calders, K., Labrière, N., & Dubayah, R. (2018). Distinguishing vegetation types with airborne waveform lidar data in a tropical forest-savanna mosaic: A case study in Lopé National Park, Gabon. *Remote Sensing of Environment*, *216*, 626–634. https://doi.org/10.1016/j.rse.2018.07.023
17. Pal, M. (2005). Random forest classifier for remote sensing classification. *International Journal of Remote Sensing*, *26*(1), 217–222. https://doi.org/10.1080/01431160412331269698

18. Thenkabail, P. S., Enclona, E. A., Ashton, M. S., & Van Der Meer, B. (2004). Accuracy assessments of hyperspectral waveband performance for vegetation analysis applications. *Remote Sensing of Environment*, *91*(3), 354–376. https://doi.org/10.1016/j.rse.2004.03.013

19. Tang, H., Armston, J., Hancock, S., Marselis, S., Goetz, S., & Dubayah, R. (2019). Characterizing global forest canopy cover distribution using spaceborne lidar. *Remote Sensing of Environment*, *231*, 111262. https://doi.org/10.1016/j.rse.2019.111262

20. Ustin, S. L., Gitelson, A. A., Jacquemoud, S., Schaepman, M., Asner, G. P., Gamon, J. A., & Zarco-Tejada, P. (2009). Retrieval of foliar information about plant pigment systems from high resolution spectroscopy. *Remote Sensing of Environment, 113,* S67–S77. https://doi.org/10.1016/j.rse.2008.10.019

Appendix A : Figures

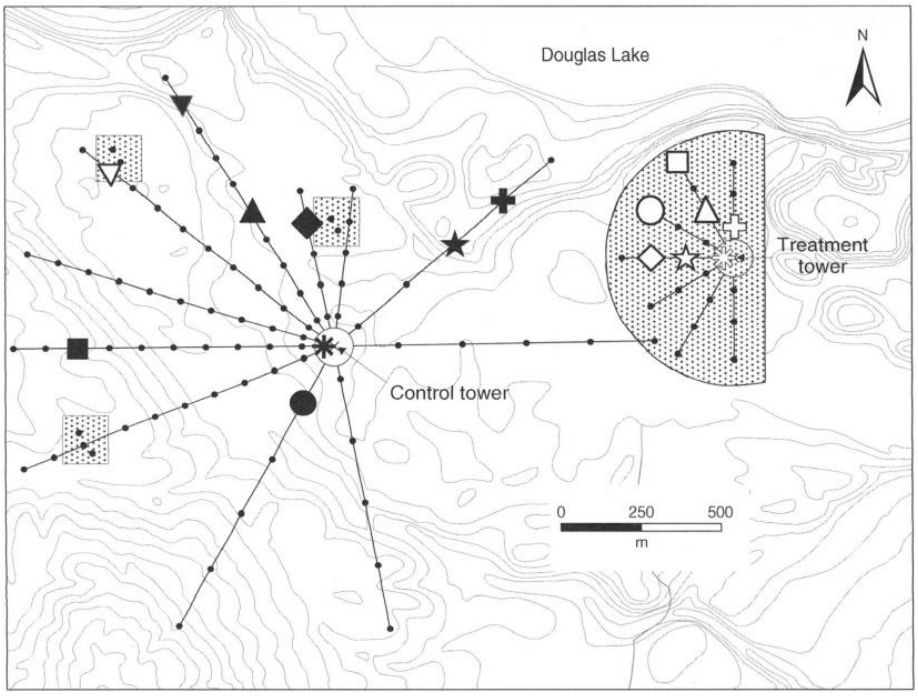

Figure 1. UMBS Flux Tower Plot. Market area around the treatment tower indicates disturbed forest region.

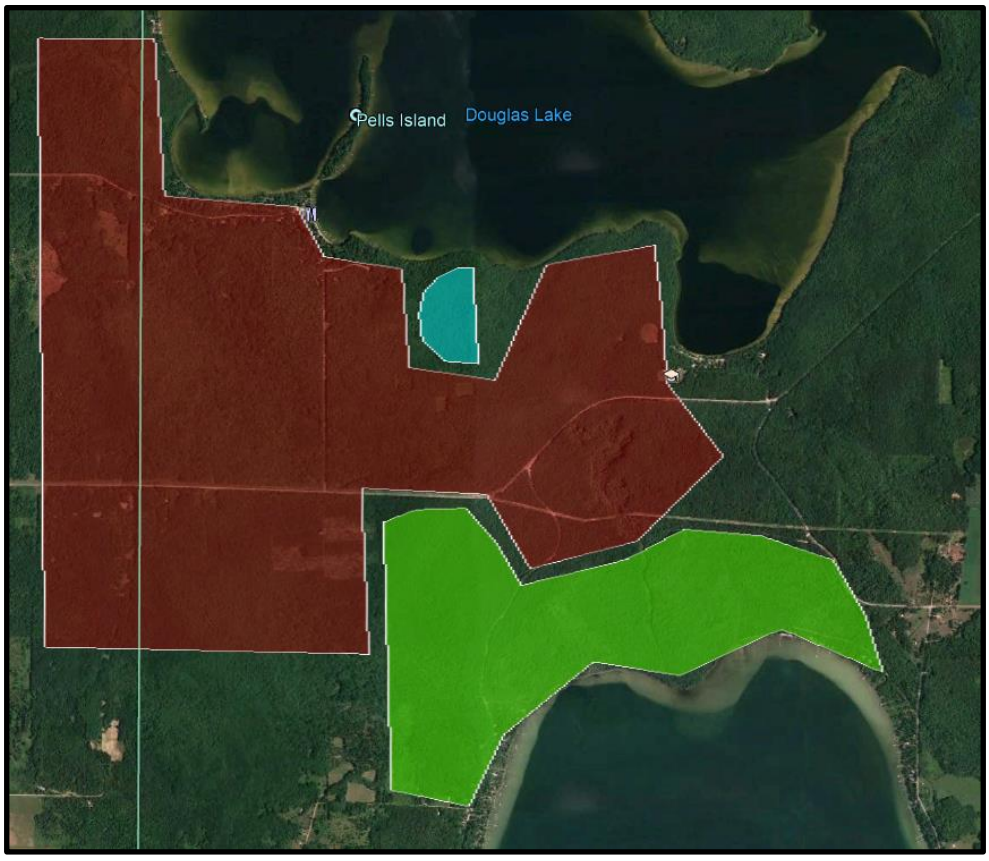

Figure 2. Successional Classification Scheme over UMBS

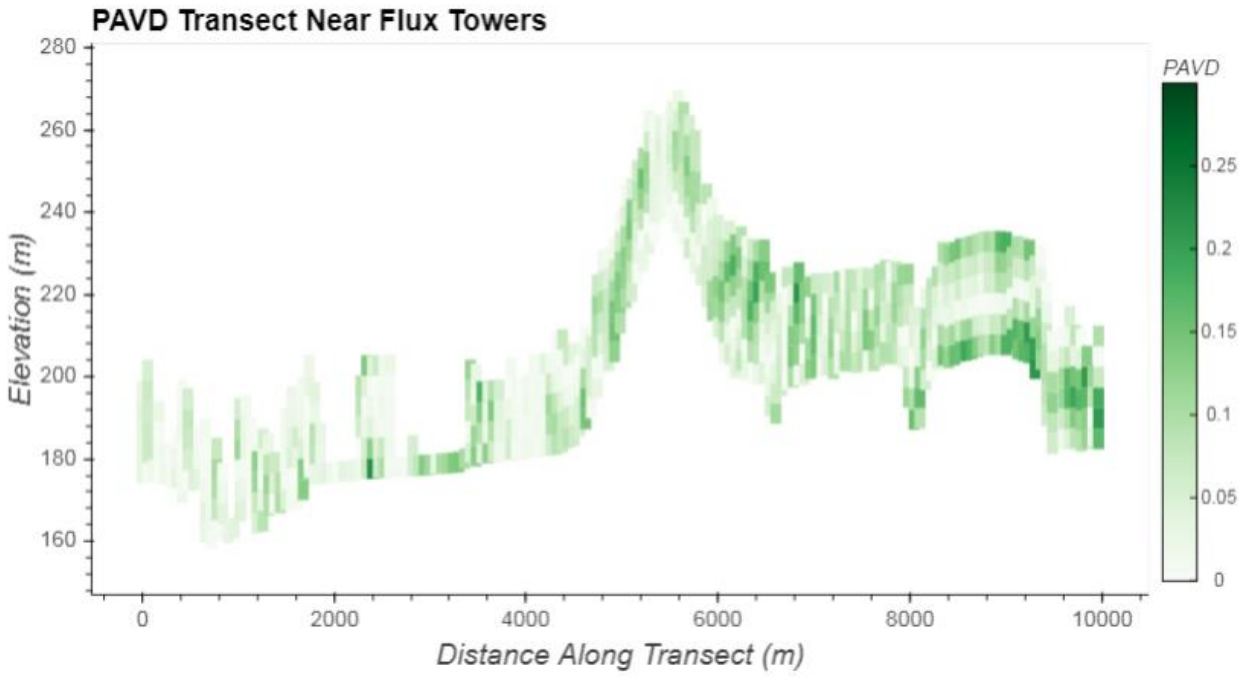

Figure 3. Sample PAVD Profile Transect. This transect does not correspond to any path over UMBS.

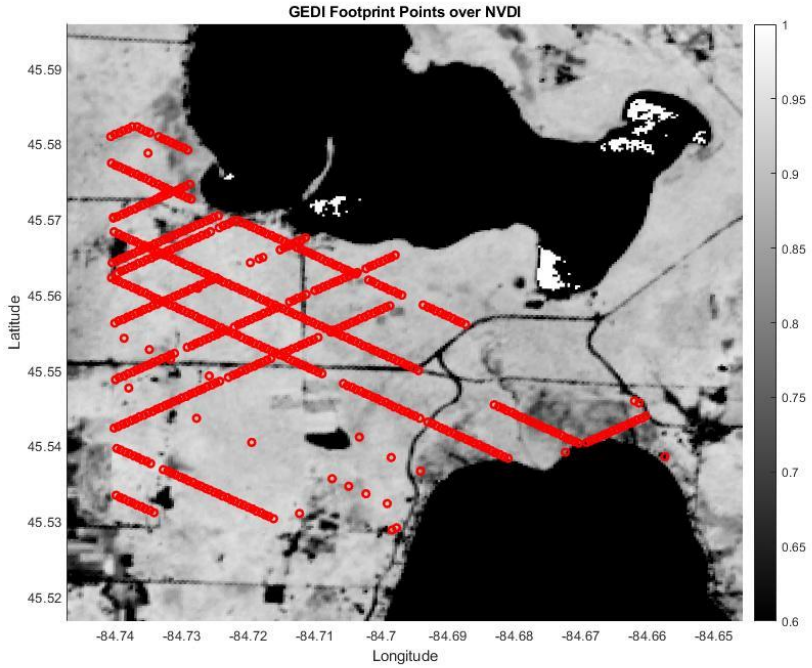

Figure 4. GEDI Footprint Locations over UMBS. Surface colorized by NDVI calculated over August 11th DESIS acquisition.

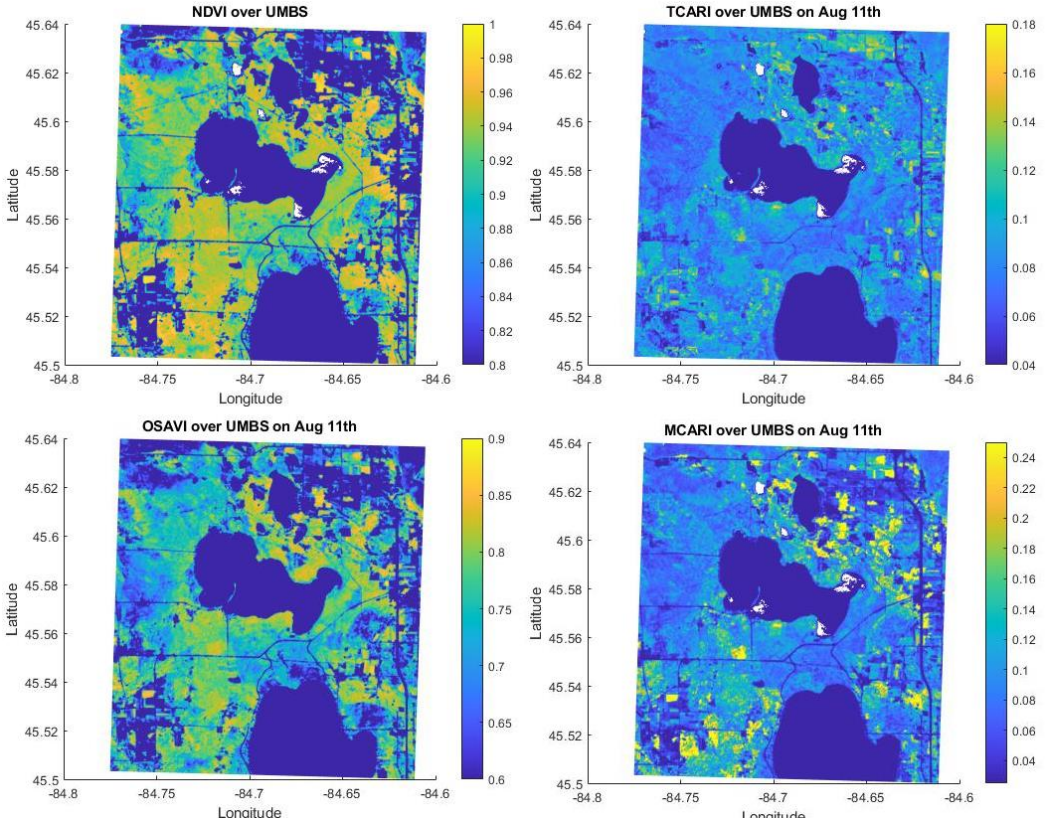

Figure 5. Four Vegetative Indices over UMBS, calculated over August 11th DESIS acquisition.

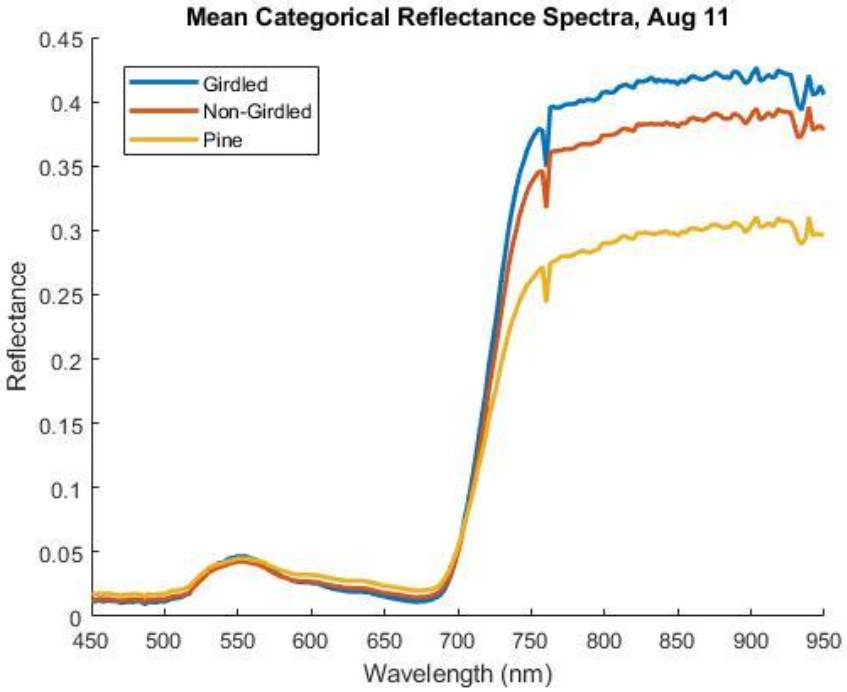

Figure 6. Mean spectra from classified footprints over UMBS on August 11th DESIS acquisition

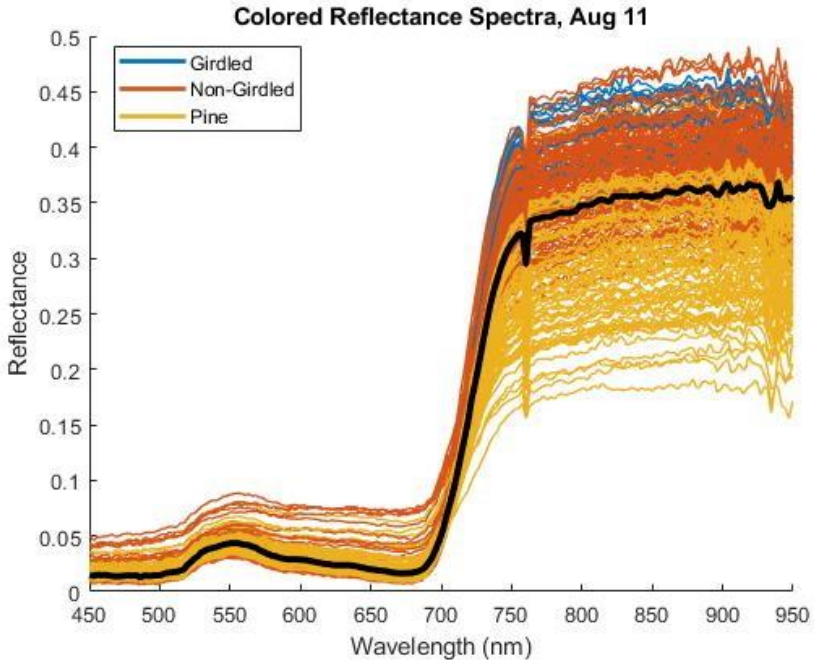

Figure 7. All reflectance spectra colorized by classification from August 11th DESIS acquisition. Black line depicts the average spectra of all points.

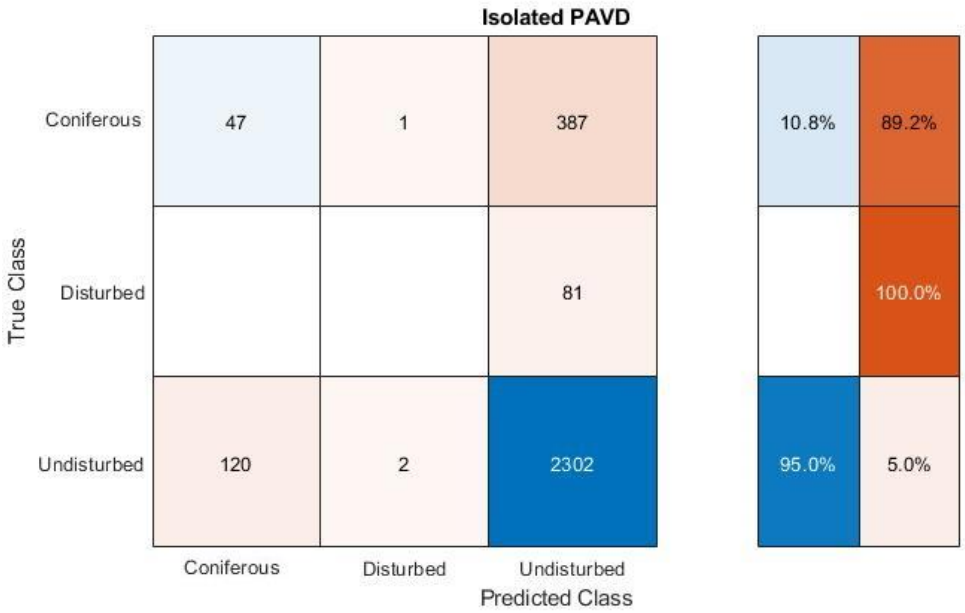

Figure 8. Isolated PAVD Training Confusion Chart

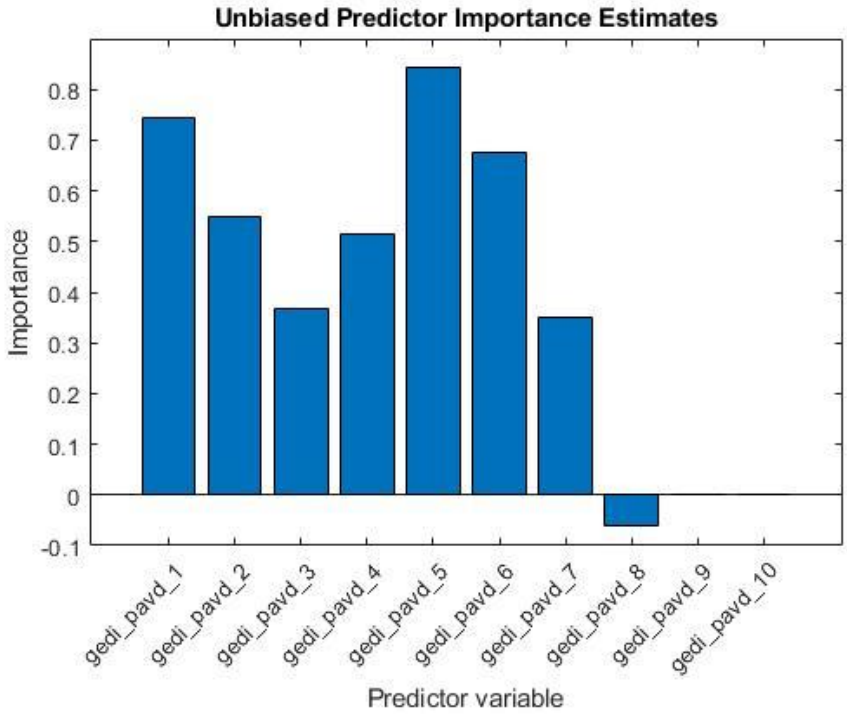

Figure 9. Predictor Importance of PAVD Profile Bins. Binning starts at 1 as 0m-5m.

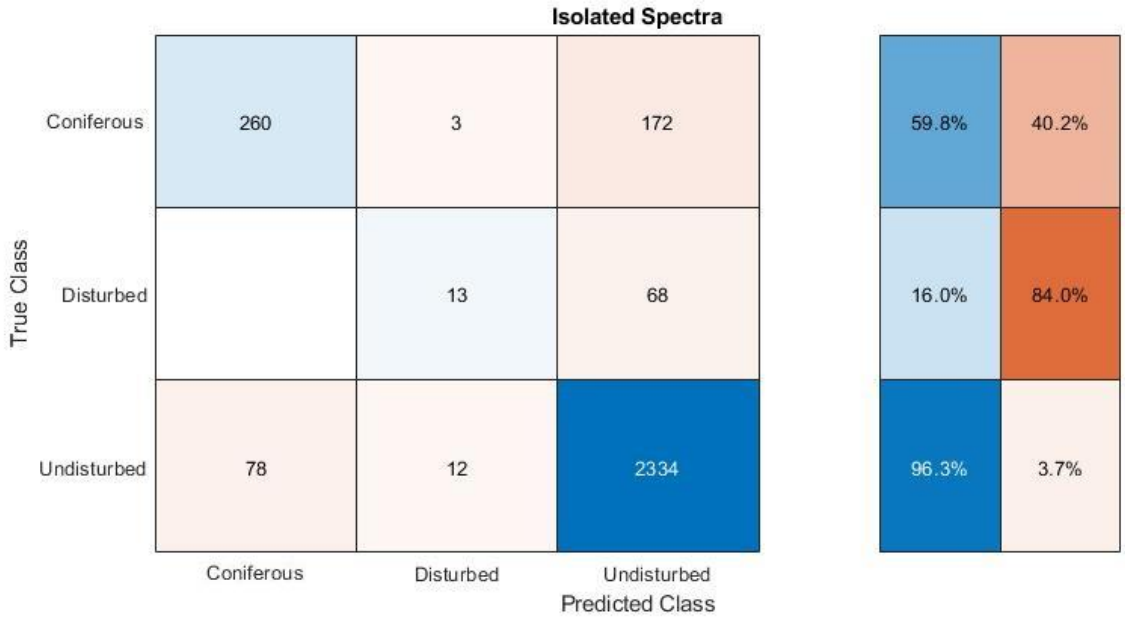

Figure 10. Isolated Training over Spectra Confusion Chart

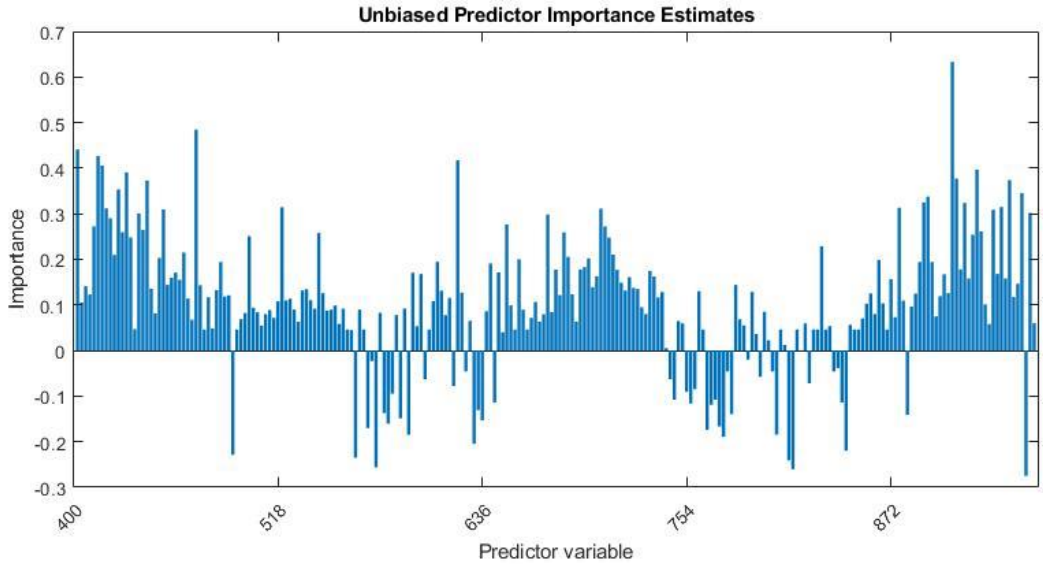

Figure 11. Predictor Importance of Spectral Bins. 235 bins varying between 400nm and 1000nm.

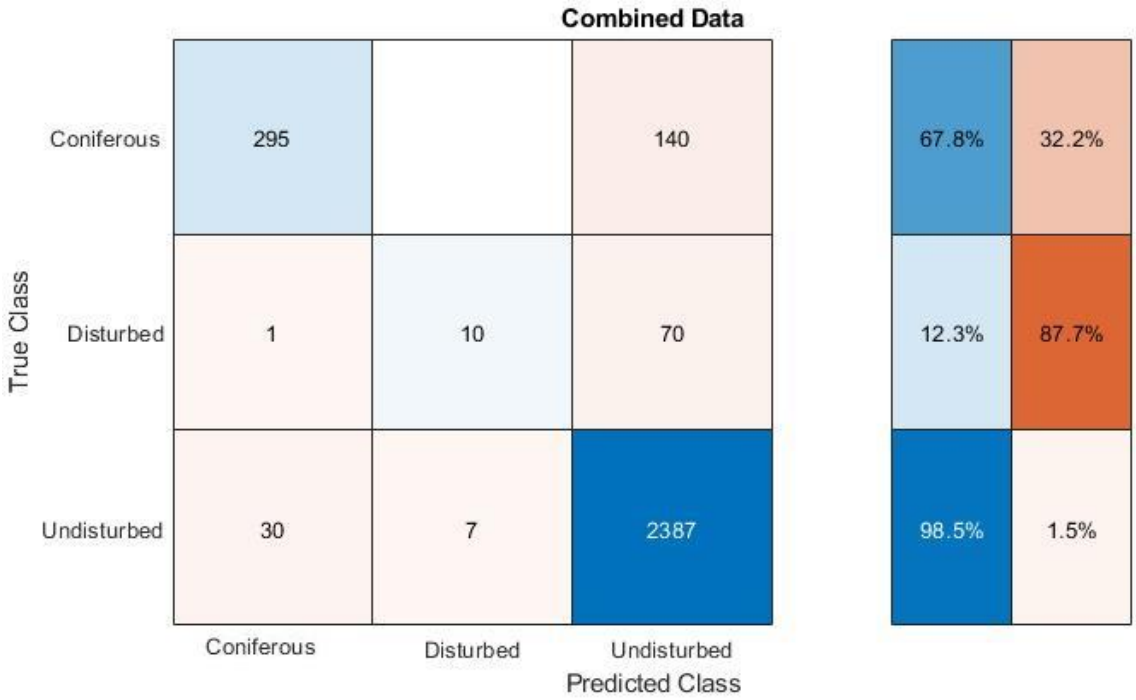

Figure 12. Complete Dataset Training Confusion Chart

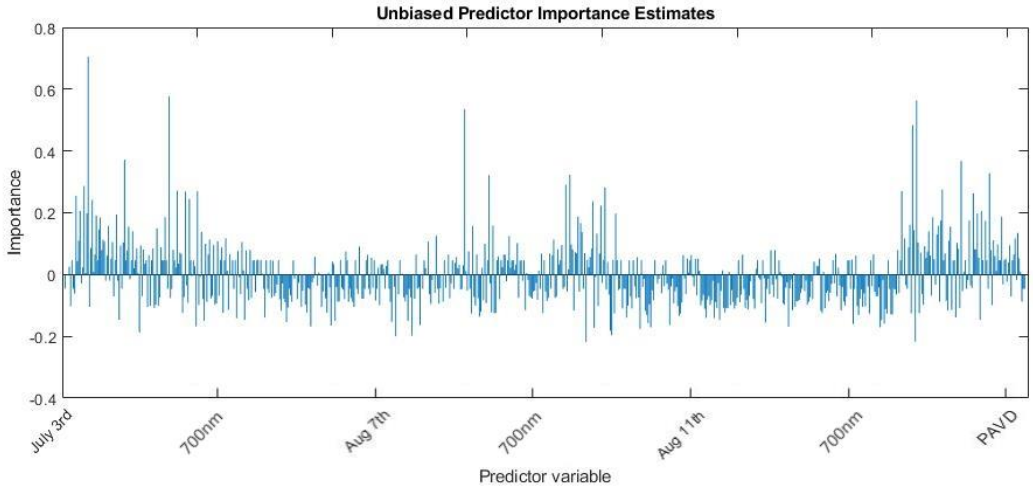

Figure 11. Predictor Importance of Combined Feature Vector. 715 features from 3 sets of 235 spectral bins and 10 PAVD profile bins.